# The facility to control the production of shashlik type electromagnetic calorimeter

S.Barsuk[a], S.Belikov[b], A.Denisov[b], A.Golutvin[a],
V.Kochetkov[b], V.Mayatski[c], E.Novikov[a], D.Rusinov[a], V.Rusinov[a],
V.Semenov[b], A.Soldatov[b], S.Shuvalov[a], E.Tarkovski[a], V.Zharkov[c]

**Abstract**

An extensive test technique has been elaborated by ITEP/IHEP/UNIPLAST group to build electromagnetic calorimeter for HERA-$B$ experiment at DESY and to control its performance. Considered is how to modify the test procedure in view of electromagnetic calorimeter development for LHCb experiment at CERN.

## 1 Introduction

In high energy physics experiments "shashlik" electromagnetic calorimeters are now widely used. The "shashlik" technology implies a sampling scintillator/lead structure read out by plastic WLS fibers. So far this technology has been successfully developed for the HERA-$B$ experiment [1, 2] at DESY ( module production, tests and the complete system running ), the PHENIX experiment [3] at BNL ( production and extensive control system ), and the RD36 project [4] at CERN. Taking into account good

[a]ITEP, Moscow
[b]IHEP, Protvino
[c]UNIPLAST, Vladimir

energy resolution, fast response time and reliability of the "shashlik" calorimeter, as well as the experience accumulated at other experiments, the same technology has been accepted for electromagnetic calorimeter production in the LHCb experiment [5].

Below the emphasis is made on test procedure elaborated and proved for the HERA-$B$ experiment. The changes and modifications needed are discussed in view of LHCb electromagnetic calorimeter to be built.

## 1.1 HERA-$B$ calorimeter

HERA-$B$ detector is optimized to measure $CP$ asymmetry in the decay $B \to J/\psi K_S$ followed by $J/\psi \to l^+ l^-$, while both electrons and muons contribute to the latter mode. Lepton reconstruction and identification is also very important in the tagging technique to establish the initial flavour of decaying $B$ meson.

Electromagnetic calorimeter plays an important role in the electron identification and first level trigger in the HERA-$B$ experiment. It is mainly designed

- to provide a pretrigger signal, which initiates first level trigger search;
- to discriminate *hadrons* against $e^{\pm}$ at the level of $\sim 100$.

This task imposes the following requirements on the performance of HERA-$B$ calorimeter.

- **Acceptance requirements** are determined by the physics task. To detect both electrons from $J/\psi$ and tagging electrons the calorimeter should be effective for $\theta_x < 220\ mrad$ and $\theta_y < 160\ mrad$. The geometrical acceptance [1] is 70% ( 83% ) for $J/\psi$ ( tagging ) electrons. The acceptance loss is caused mainly by the inner hole, which is anyhow inefficient in the tracker system.

[1] The values quoted imply both $e^+$ and $e^-$ to be detected.

- **Time requirements.** The time between two subsequent bunches at HERA is 96 $ns$. Thus the signal collection must proceed well within this time interval.

- The fine **transverse segmentation** improves the discrimination between electrons and charged hadrons overlapping with photons from $\pi^0$ decays. It also improves spatial resolution and the capability to separate two showers.

- **Energy resolution** should be sufficient to provide the required $e/\pi$ separation and the accurate measurement of photon energies.

- **Radiation resistance.** The annual radiation dose of up to 0.2 $Mrad$ can be reached in the middle calorimeter zone [2].

## 1.2 LHCb calorimeter

LHC will be by far the most copious source of $B$ mesons, due to the high $b\bar{b}$ cross section and high luminosity. The LHCb detector is designed to exploit the above LHC features. The experiment will operate with an average luminosity of $2 \times 10^{32}\ cm^{-2}s^{-1}$ which should be obtained from the beginning of LHC operation, and achieve the production rate of $10^{12}\ b\bar{b}$ pairs per year of data taking.

LHCb experiment is aimed at the precision studies of $CP$ asymmetries and of rare decays in the $B$ meson systems.

$B_d^0 \to \rho^0\pi^0 \oplus tag$, $B_d^0 \to \rho^+\pi^- \oplus tag$, $B_d^0 \to J/\psi K_S^0 \oplus tag$, $B_d^0 \to K^{*0}\gamma$ and $B_s^0 \to J/\psi\phi \oplus tag$ are the decays that illustrate the role of electromagnetic calorimeter in the LHCb experiment. Efficient $\pi^0$'s reconstruction in the wide range of momentum spectrum, discrimination between electrons and charged hadrons with overlapping photons, the tag electron reconstruction and the reconstruction of high energy $\gamma$'s contribute good deal of the scientific program to the experiment.

[2] The innermost calorimeter zone is composed from $W/Sc$ modules, the production and control of which were completely different from the discussed technique. Also no such modules are assumed to be used in the LHCb experiment. The outer region modules do not suffer from such a dose for the dose drops drastically with the distance from the beam pipe. For the HERA-$B$ dose map, see [2].

Electromagnetic calorimeter is a part of LHCb calorimeter system, which also comprises the preshower detector ( used to improve the identification at the trigger level ) and the hadron calorimeter. Electromagnetic calorimeter will be placed at about 12.5 $m$ from the interaction point ( Figure 2 ). The readout system of the calorimeter comprises 5952 channels, 1472, 1792 and 2688 from which belong to inner, middle and outer regions respectively.

The requirements on the LHCb electromagnetic calorimeter are as follows.

- **Acceptance.** The outer dimensions are matched projectively to those of the tracking system, $\theta_x < 300\ mrad$ and $\theta_y < 250\ mrad$. Due to the substantial radiation dose level around the beam pipe, the active calorimeter volume has a central square hole of $64 \times 64\ cm^2$. Since the event samples that high level triggers deal with, are dominated by "$b$ events", this does not lead to $B$ performance degradation.

- **Response time.** To avoid event pile-up the signal collection time should be below 25 $ns$.

- The hit density is a steep function of the distance from the beam pipe, and varies over the active calorimeter surface by two orders of magnitude. The **transverse segmentation** is optimized on the basis of best possible $\pi^0$ reconstruction efficiency and trigger performance, with a constraint of the maximum allowed cost of calorimeter ( mainly determined by the number of cells ). Calorimeter is subdivided into three, inner, middle and outer, regions, with the $40.4 \times 40.4\ mm^2$, $60.6 \times 60.6\ mm^2$ and $121.2 \times 121.2\ mm^2$ cell size respectively.

- The design **energy resolution** of

$$\frac{\sigma_E}{E} = \frac{10\%}{\sqrt{E}} \oplus 0.8\% \quad (E\ in\ GeV)$$

  provides $e/h$ separation at a level better than 100 and is adequate for $\pi^0$ reconstruction.

- **Radiation resistance.** The dose map has its maximum of up to 0.25 $Mrad$ per year of LHCb operation for the innermost modules and drops with the distance from the beam pipe. Longitudinally the radiation influences relatively small part of the calorimeter in the vicinity of shower maximum.

## 1.3 Module design

The HERA-$B$ and LHCb electromagnetic calorimeters exploit quite similar module design. Here main accent is made on the LHCb calorimeter module design, though the differences between the two calorimeters are mentioned.

The schematic drawing of the LHCb calorimeter modules is shown in Fig. 3. Inner, middle and outer section modules have similar design differing by the number of cells per module and by the fiber density. We are planning to use 9, 4 and 1 cells per calorimeter module and 16, 36 and 64 fibers per cell, for the inner, middle and outer sections respectively [3].

The module is constructed from alternating layers of 2 $mm$-thick lead, white reflecting 120 $\mu$ thickness paper ( TYVEK ) and 4 $mm$-thick scintillator tiles.

The tile is produced of polystyrene-based $PSM$-115 scintillator with the 2.5% p-terphenyl and 0.01% $POPOP$ admixtures. The concentration of scintillating dopants is tuned for the scintillator tile emission spectrum to match the absorption spectrum of WLS fiber. Scintillator tile production employs the injection moulding technique under high pressure.

The complete stack is compressed using stainless steel side covers of 100 $\mu$ thickness, pre-tensioned and welded to front and rear 1 $mm$ thick steel lids. In total, there are 66 layers resulting in a total depth of 25 $X_0$.

[3] The inner, middle and outer modules of HERA-$B$ calorimeter comprise 25, 4 and 1 calorimeter cell respectively. For the middle and outer regions, i.e. for the regions exploiting the same technology as the one discussed, $55.75 \times 55.75$ $mm^2$ and $111.5 \times 111.5$ $mm^2$ calorimeter cells are used.

In the HERA-$B$ calorimeter to improve light collection and prevent tile-to-tile crosstalk, the tile edges were aluminized. In order to that Al evaporation in vacuum by HV-induced explosion was used. For the LHCb calorimeter the tile edges will be chemically mat, which provides better diffusive reflection quality.

The light is read out via 1.2 $mm$ diameter WLS fibers penetrating the entire module, with PM. The fibers belonging to each calorimeter cell are bundled at the end of the module and polished. The fibers form a loop in the front part of the module for large module sizes, where loop is possible without significant light losses. Such fiber "pairing" is not possible for small module sizes ( i.e. small curvature radii of fibers ), e.g. for inner section modules for both HERA-$B$ and LHCb experiments. In this latter case, the fibers are cut, polished, and aluminium mirror is made on the fiber front edge with the technique of sputtering.

# 2 Performance measurements for HERA-$B$ calorimeter

The final goal of all the test measurements is to construct the calorimeter modules with similar response and designed performance. This implies a detailed control at each step of module production, starting from the control of raw material and up to characteristics studies of the assembled module.

An extensive test procedure has been elaborated to prove the technique, and to monitor material and module performance. The most attention has been paid to

- monitor the scintillator composite and response;
- control module performance.

The idea of all control measurements described below, is to compare the result of measurement ( value, spectrum, etc. ) with that obtained for the working standard.

Working standard is substance, tile or module, the performance of which is carefully proved by the extensive studies from spectroscopy analysis and up to the beam tests.

## 2.1 Raw material control

The most important at the stage of raw material treatment is the polystyrene and p-terphenyl quality control.

### 2.1.1 polystyrene quality control

As we have mentioned above, the polystyrene -based $PSM$-115 plastic, which shows similar radiation hardness [6], is used instead of pure polystyrene .

Two tests are made to control the quality of polystyrene .

First one is based on infrared spectroscopy technique, which is developed to analyze composition of organic substances. The idea is that in the method different chemical bonds correspond to different resonance frequencies. Then the frequency spectrum is compared to the standard one. Fig. 4 shows the infrared spectra for the two samples of $PSM$-115 plastic, only the minor difference is seen. The pure polystyrene spectrum shows no peak in the region indicated by arrow.

Another application of the technique consists in identification of the extraneous admixture present in polystyrene sample. The specimen is taken out mechanically and dissolved in the e.g. chloroform. The spectrum of this solution is compared to the standard spectrum of polystyrene , and to other standard spectra.

The other one is the "transparency" control, i.e. the response from polystyrene vs. wavelength of incoming light, measured with the spectrophotometer. The measurements are carried on with the spectrophotometer MPS-500 ( Shimadsu, Japan ) using the two-beams method. Thanks to the high apparatus sensitivity, measurements could be done either for a single tile or for rouleau of tiles.

Each tile is measured in 10 points distributed along its surface. Special attention has been paid to the transparency for the light with $\lambda = 420\ nm$, because the scintillator emits the light of this wavelength. To account for losses due to the partial reflection, the reference value measured at $\lambda = 590\ nm$ is subtracted [4].

### 2.1.2 p-terphenyl quality control

First p-terphenyl sample is subjected to the infrared spectroscopy test ( see section 2.1.1 ).

Next come two methods – gas and liquid chromatography [5]. Both are quantitative and probe chemical composition and concentration of components using the measurements of time delay and amplitude of separated chemical compounds.

And the last test to control p-terphenyl quality is the transparency studies with the spectrophotometer, as in section 2.1.1. Controlled is the spectra difference between test and reference samples.

## 2.2 Scintillator tile control

After being ensured in raw material quality [6] one can produce a scintillator plate. Next is to control scintillator plate performance, which is done in three steps.

Spectrophotometer control ensures transparency to the blue ( 420 $nm$ ) light. Fig. 5 shows the tile-to-tile transparency variations. The individual value $\hat{\mu}$ is the average over the values $\frac{I_{590}-I_{420}}{I_{590}}$, as measured at 5 different points laterally distributed over the tile. $I_{420}$ and $I_{590}$ stand here for the transparency of a tile for 420 and 590 $nm$ light correspondingly. The mean of 5.8% of 420 $nm$ light is lost with the r.m.s. of the

[4] At this wavelength the absorption is closed out completely.

[5] Liquid chromatography has been developed to analyze high-molecular compounds.

[6] In fact the technique to determine the dye dopant concentration in the produced scintillator tile, with spectrophotometer, has been elaborated. This technique appeared to be time- and work-consuming, and has been used to establish other control methods only. Also reasonable is to take away material with inadequate quality at the early stage, which saves other components.

distribution of 0.5%. The transparency variations within a tile over its surface could be estimated by the $\sqrt{\hat{\sigma}^2}/\hat{\mu}$ value ( see Fig. 6 ), where $\hat{\sigma}^2$ is the variance of one tile measurements.

The setup of the next test resembles a hedgehog, and represents a scintillator plate and fibers coming through its holes. The plate is irradiated with $^{90}Sr$ radioactive source, and measured is the response from fibers ( via PM ).

An individual measurement comprises the measurement of dark current, i.e. noise plus fiber response to the irradiation, and the measurement of current from complete "hedgehog" ( scintillator tile plus fibers ). The result of the test is the difference of the two measured values. It is then compared to the standard tile. Tiles with the difference of less than 5% from the standard value, are accepted for further control.

Scintillator tile is subjected to the same "hedgehog" test after aluminization ( mating ) of edges. This is done with a special care for two reasons. One is that the quality of edge aluminization ( mating ) influences significantly the light yield from a tile. Besides tested here is the end product with a predefined characteristics, followed by the assembly procedure only. Fig. 7 shows the results of the "hedgehog" test as averaged for groups of three tiles. Shown is the light yield relative to that of a reference tile [7]. The tiles with $LY > 0.93 \cdot LY_{ref}$ ( corresponding region is to the right from arrow ) were then used for module assembly. The r.m.s. for the remaining sample is $\approx 0.09$.

The analysis shows that the tile quality crucially depends on the edge coating quality, and there is only a minor dependence on the transparency properties.

## 2.3 Module performance measurements

The energy resolution of middle section modules was studied with the electron beam at DESY [8]. The electron momentum range of $1 \div 5\ GeV/c$ was used for measurements.

[7] The reference tiles were taken from a bunch of tiles successfully passed the beam measurements. One reference tile substitutes another after the aging of the latter one becomes visible.

[8] For more details see e.g. [7]

The experimental results obtained ( filled dots in Fig. 8 ) are in good agreement with EGS4 simulations ( stars in Fig. 8 ). The simulation results can be fitted with a resolution function of

$$\frac{\sigma_E}{E} = \frac{9.5\%}{\sqrt{E}} \oplus 1\% \ .$$

The measurements are fully consistent with this form.

The energy resolution of 80 middle section modules was measured with 3 $GeV/c$ electrons. The resolution spread was found to be about 6%. The uniformity map was studied by comparing the ratio of responses in center and near the border of a cell. The mean value of the ratios was found to be 0.985 with a 2% variation.

The cell-to-cell non-uniformity in the middle section modules was studied with protons of 2.5 $GeV/c$ momentum at ITEP. The cells turned out to be identical within 10% $r.m.s.$ [9].

All these module studies show well the reproducibility of the production technology.

# 3 Control program for LHCb calorimeter

The control results obtained for HERA-$B$ electromagnetic calorimeter provides an exceptional base to elaborate the control system for LHCb . All the material studies of polystyrene and p-terphenyl , including the infrared spectroscopy technique, spectrophotometer analysis, gas and liquid chromatography, is extremely important as the input control for each bunch of material.

As the control of produced tiles optimal is the "hedgehog" test. This is to be done for each bunch of tiles [10]. The mating is to be extensively studied as a new development by the "hedgehog" test.

In order to check module assembly ( tile/Pb/fibre ) and forming a fiber bundle quality,

[9] The 7.5% value could be achieved by using a hot wire to cut the fiber ends.

[10] Typically 1 out of 5 tiles is tested.

one should check the module response to cosmic particles, or to radioactive source, or to the laser light. With e.g. the cosmic particle fluxes one ensures the required module performance and module-to-module variations of the light yield. Trigger based on the scintillator counters provides the two-coordinate measurements of a track in front of and behind the module. The ADC spectrum could be used to determine the number of photoelectrons per MIP. As far as routine quality control is concerned, all the modules will pass the cosmic test in the scheme, where individual module is placed horizontally, and trigger is organized with the coincidence of above and below scintillator counters. By using the only calibrated PM for the cosmic test, one achieves the accuracy of $1.5 \div 2.0\%$ within a half an hour time scale.

And finally, the selective beam studies of the completed module response, uniformity, energy and spatial resolution will ensure the overall module performance.

# 4 Summary and outlook

An extensive test program for HERA-$B$ electromagnetic calorimeter modules has been elaborated. The technique has been proved by module beam tests.

Being well-grounded on the experience collected with HERA-$B$ calorimeter production and tests, the control program for LHCb calorimeter production is proposed.

# References


[1] HERA-B Collaboration, HERA-B Proposal, DESY-PRC 94/02 May 1994.

[2] HERA-B Collaboration, HERA-B Design Report, DESY-PRC 95/01 January 1995.

[3] Bazilevsky A. *et al*, IEEE Transactions on Nuclear Science v.43, No.3 (1996).

[4] J.Badier *et al*, "Shashlik Calorimeter: Beam Test Results", NIM A348 (1994) 74-86.

[5] LHCb Collaboration, LHCb Technical Proposal, CERN LHCC 98-4 LHCC/P4 20 February 1998.

[6] CMS Collaboration, Technical Proposal, CERN LHCC 94-38 LHCC/P1 15 December 1994.

[7] E.Tarkovsky, "The HERA-$B$ electromagnetic calorimeter", Nucl.Instrum.Meth. A379 (1996) 515.

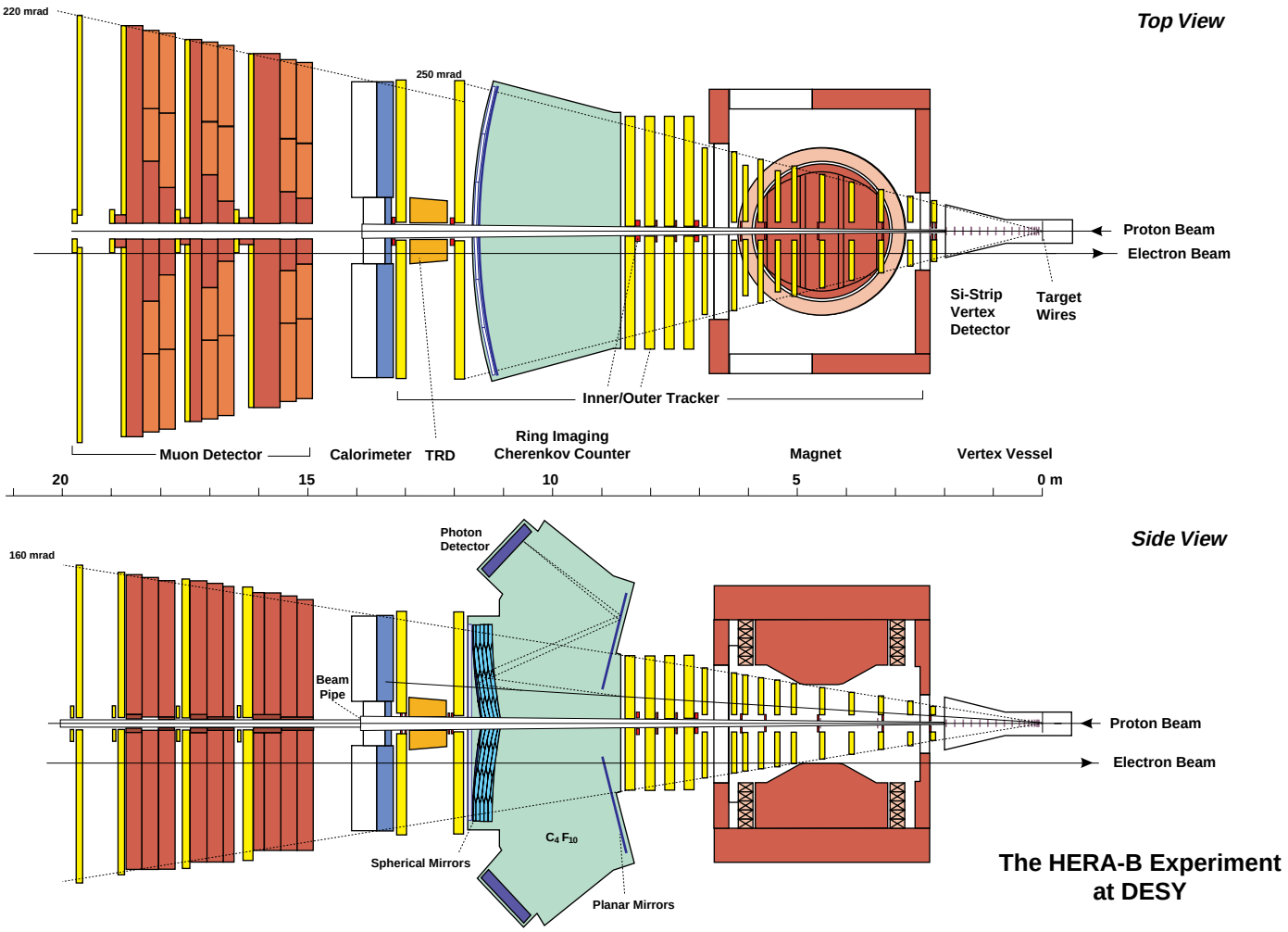


Figure 1: *HERA-B detector*

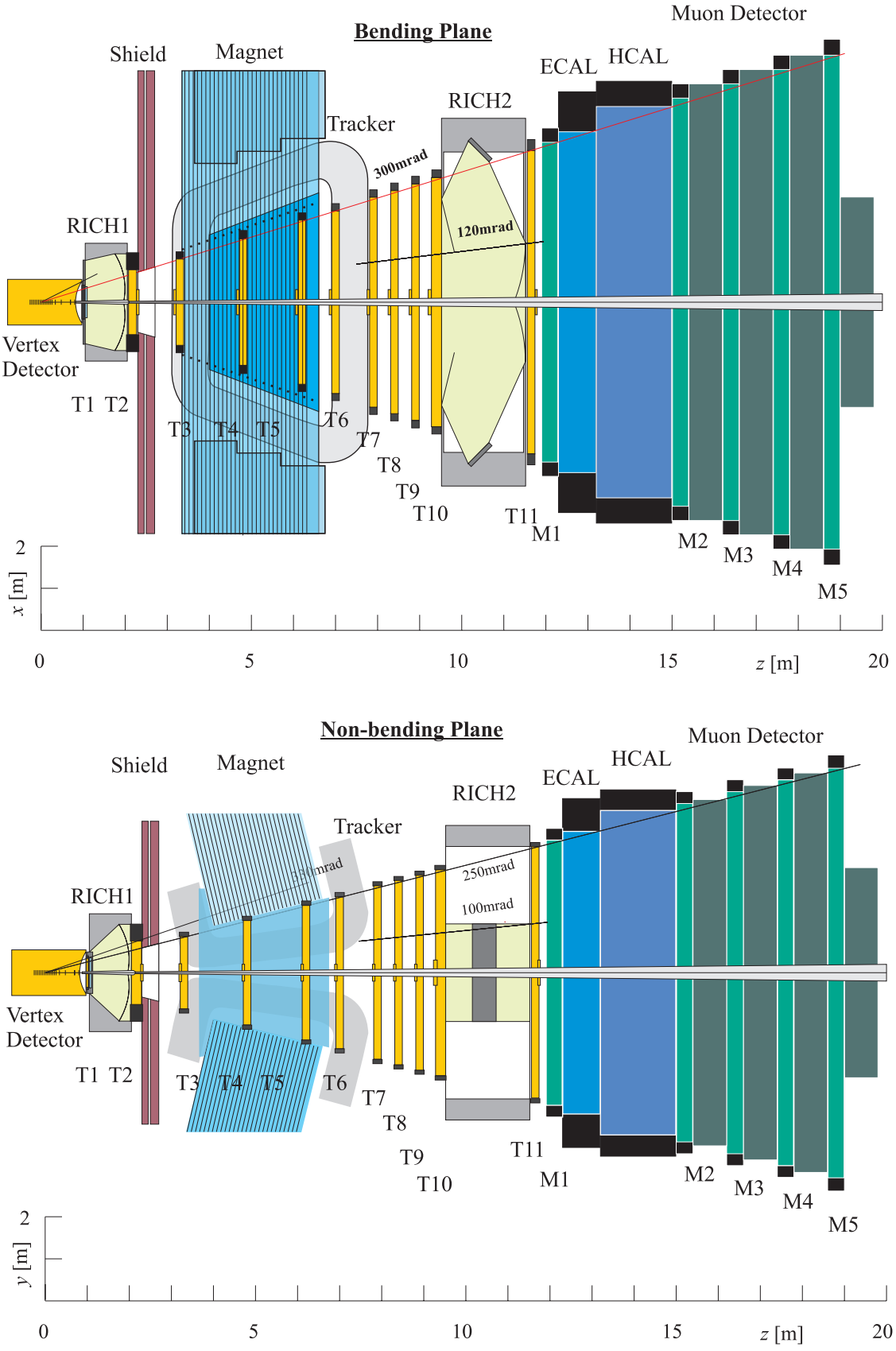


Figure 2: *LHCb detector*

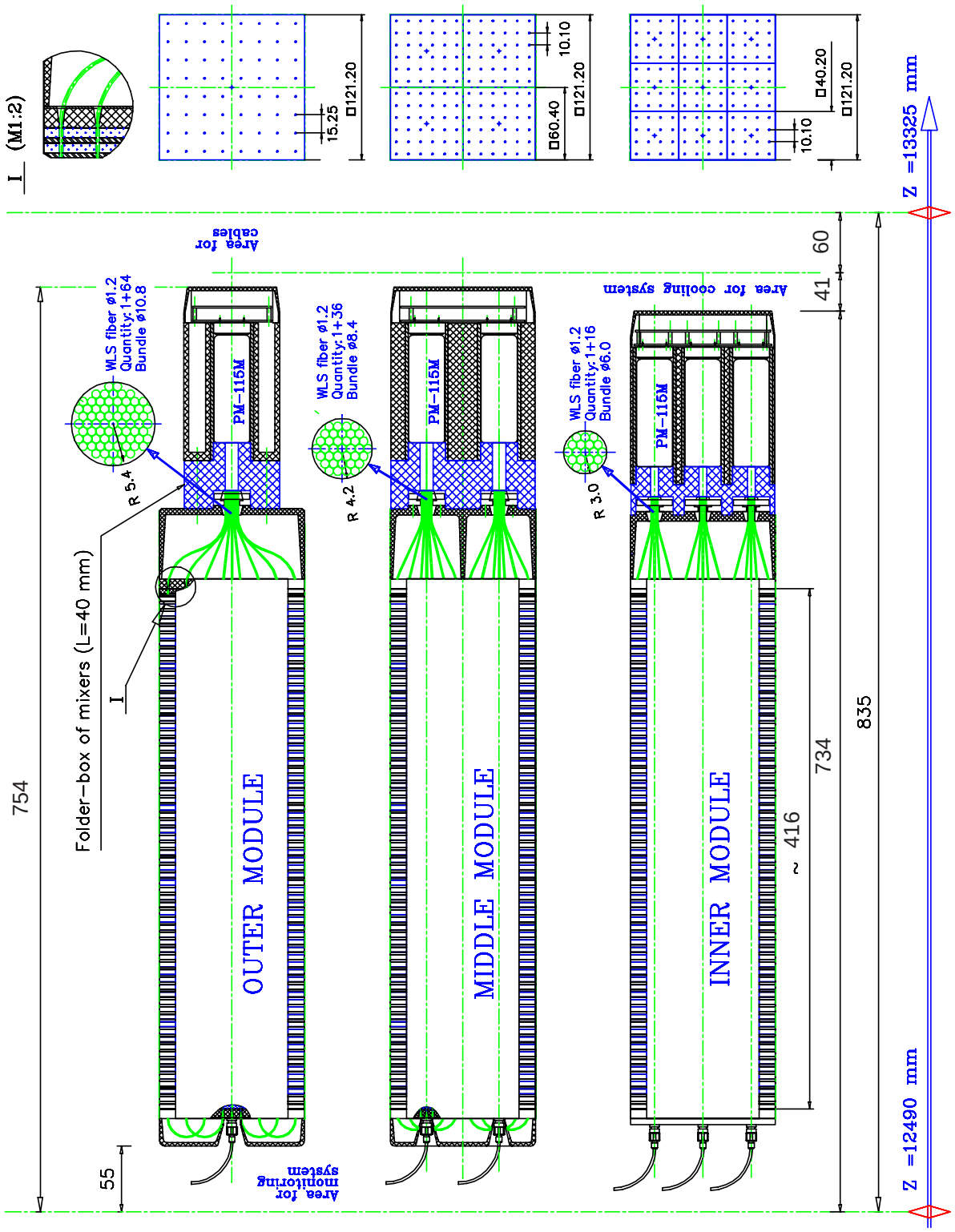


Figure 3: *LHCb electromagnetic calorimeter modules for inner, middle and outer sections. At the monitoring side shown are transport fibers, connectors, fiber loops ( if any ) and plastic covers. At the read-out side shown are fiber bundles, PMs and their bases. Also shown are area for splitters, space for cooling system and for cabling, and the related mechanics*

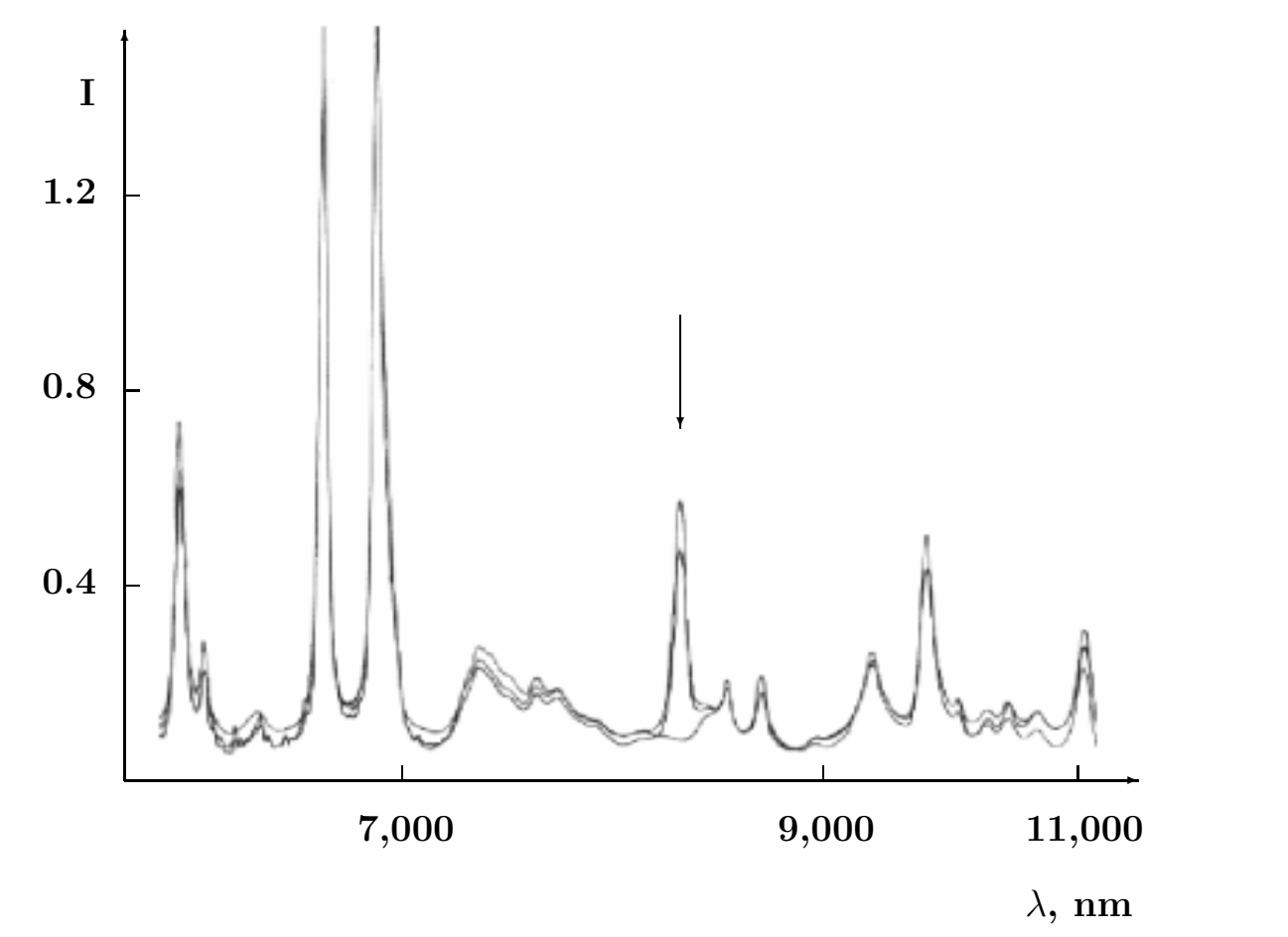


Figure 4: *The infrared spectra for two samples of PSM-115 plastic. The pure polystyrene spectrum shows no peak in the region indicated by arrow*

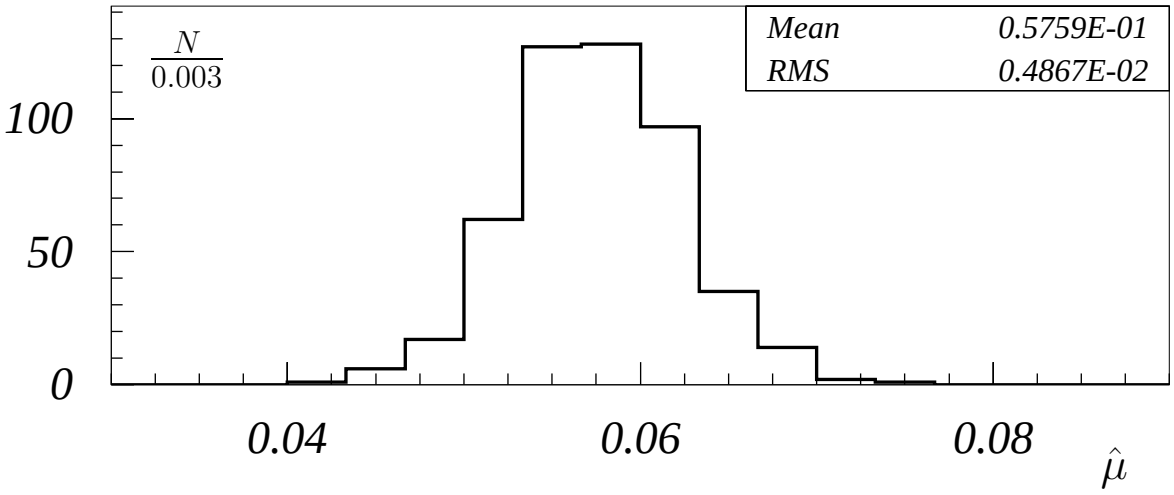


Figure 5: *Tile transparency measurements accomplished with spectrophotometer.* $\hat{\mu}$ *is an average over the values* $\frac{I_{590}-I_{420}}{I_{590}}$*, as measured at 5 points distributed over the tile surface. For details see the text*

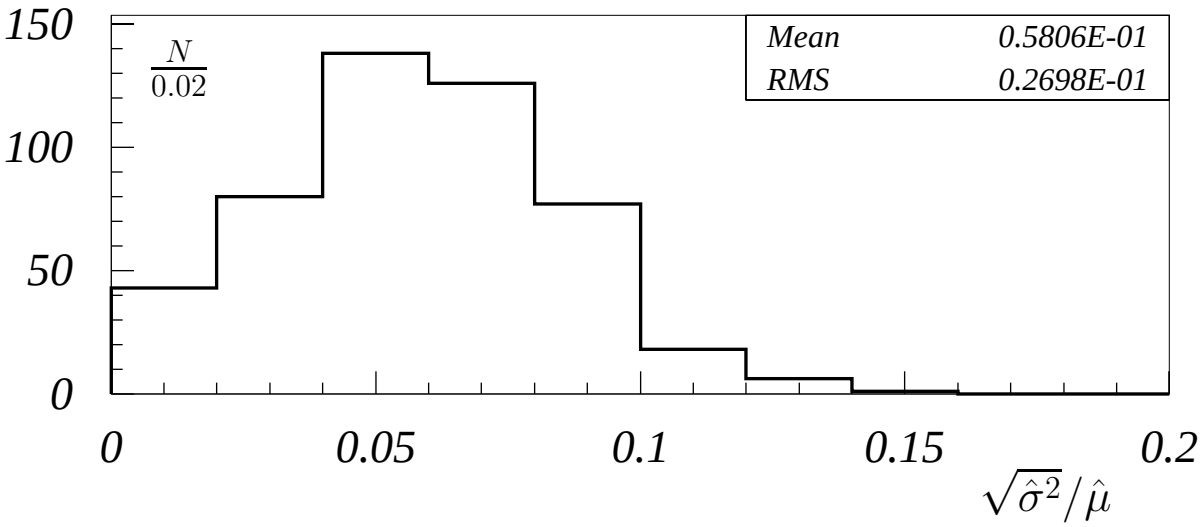


Figure 6: *Tile transparency measurements accomplished with spectrophotometer.* $\hat{\mu}$ *and* $\hat{\sigma}^2$ *are the average and variance over the values* $\frac{I_{590}-I_{420}}{I_{590}}$*, as measured at 5 points distributed over the tile surface. For details see the text*

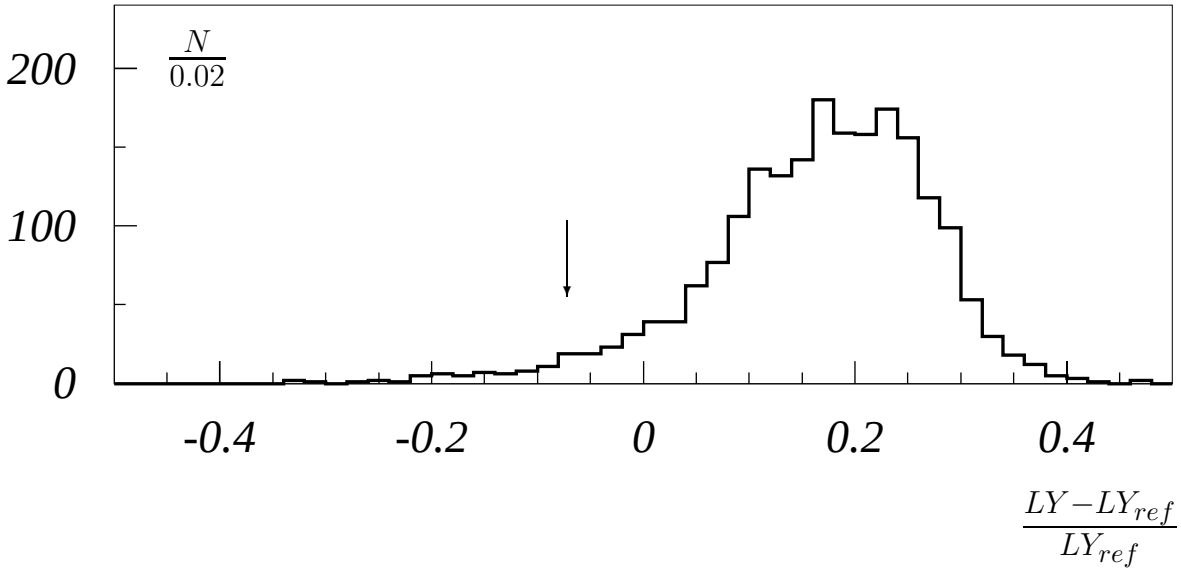


Figure 7: *Results of the "hedgehog" test as measures for groups of three tiles. Shown is the light yield relative to that of a reference tile. The r.m.s. for the tiles used for module assembly ( $LY > 0.93 \cdot LY_{ref}$, corresponding region is to the right from arrow ) is* $\approx 0.09$. *For details see the text*

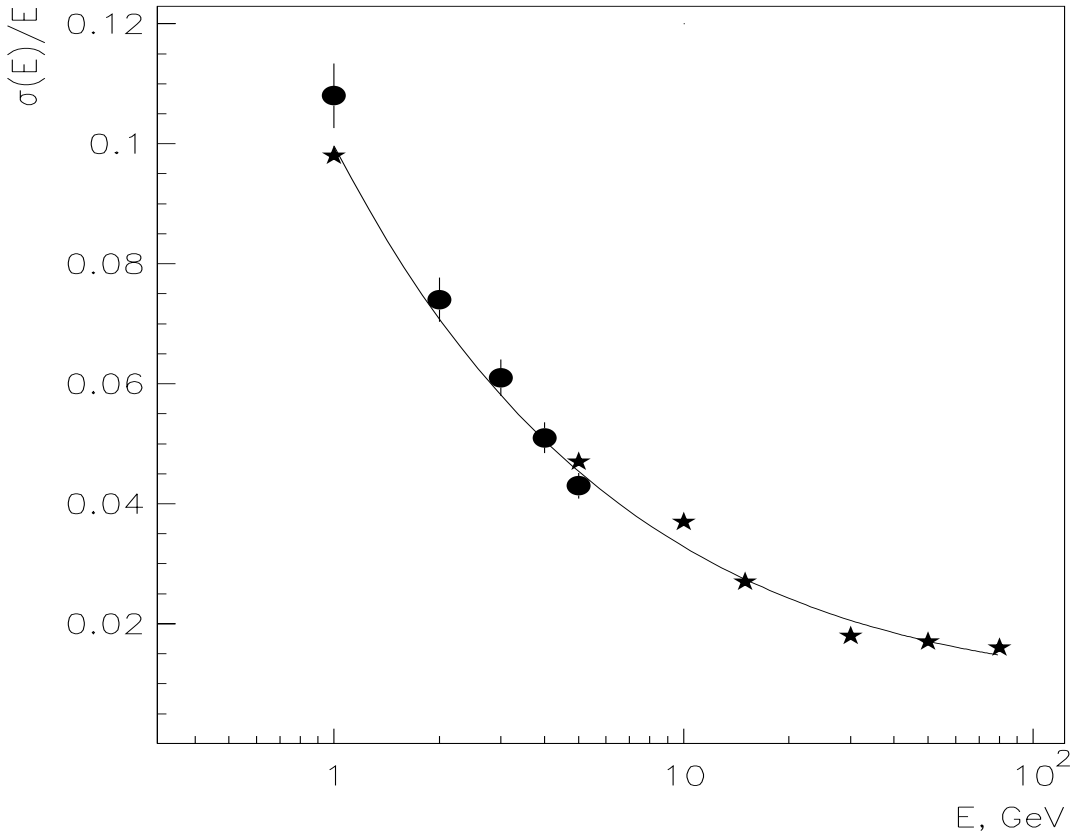


Figure 8: *Energy resolution for middle section module. Dots with errors stand for measurement results, stars – for EGS4 simulations*